Boosting electrocatalytic nitrogen reduction to ammonia in alkaline media

Guangzhe Li†, He Lin†, Zhefei Pan, Yun Liu, Liang An*

Department of Mechanical Engineering, The Hong Kong Polytechnic University, Hung Hom, Kowloon, Hong Kong SAR, China

† Equal contribution.

*Corresponding author.

Email: liang.an@polyu.edu.hk (L. An)

Abstract

Electrochemical ammonia synthesis is a promising alternative technique to traditional Haber-Bosch process, capable of converting nitrogen to ammonia at ambient conditions and can be driven by intermittent energy. However, it generally requires high overpotential for nitrogen dissociation due to the stable triple bonds of nitrogen molecules, resulting in a poor ammonia yield rate. Tailoring the electrolyte-ion composition is a promising approach to facilitate nitrogen dissociation by optimizing the local reaction environment near the electrode toward ammonia production. In this study, the effect of anions in the electrolyte composition on electrocatalytic nitrogen reduction to ammonia is investigated. It is found that a lower onset potential for nitrogen reduction (-0.2 V vs. RHE) and a higher ammonia yield rate (6.69×10^{-11} mol cm^{-2} s^{-1}) are achieved in the electrolyte containing OH^- anions, compared to singly charged anions of Cl^- and SCN^- when using an electrode made of commercial Au/C electrocatalysts. In addition, current density contributed by nitrogen reduction achieved in the high-pH electrolyte ($pH\geq13$) shows around three-fold increase compared to that in low-pH electrolyte ($11\leq pH\leq12$). Such performance enhancement is possibly attributed to the appearance of hydronium ions (H_3O^+) in high-pH electrolyte, which facilitates nitrogen dissociation by strengthening protonation ($*N_2 + 6H_3O^+ + 6e^- \rightarrow * + 2NH_3\cdot H_2O + 4H_2O$).

Keywords: Ambient ammonia synthesis; Nitrogen reduction reaction; Highly concentrated hydroxide ions; Hydronium ions; Anions.

1. Introduction

Ammonia, a globally essential chemical, has broad applications for synthesizing fertilizers and drugs[1,2] and can serve as a transportation fuel to generate electricity. It is generally produced by Haber-Bosch method[2] in industry, which converts atmospheric nitrogen and hydrogen to ammonia using a metal-based catalyst under extremely high temperature (500 - 600 ^{o}C) and pressure (300 - 400 atm).[3] To reach such harsh reaction condition, it consumes massive energy, about 1 % global fossil fuels annually. The consumption of fossil fuels leads to energy crisis and environmental burdens due to CO_2 mission. In response to these issues, electrochemical nitrogen reduction provides a promising alternative approach for ammonia synthesis. It is capable of converting nitrogen and water to ammonia and oxygen in aqueous solution under ambient condition, which can be driven by the intermittent electrical energy.[4] Normally, this electrochemical process is conducted in an electrochemical cell, which contains a cathode for nitrogen reduction, an anode for water oxidation and a membrane for ion transfer. Although promises, the ammonia yield rate ($< 3.0 \times 10^{-10}$ mol cm^{-2} s^{-1}) and Faradaic efficiency (< 20 %) for electrochemical ammonia synthesis via nitrogen reduction are still poor, far away from the targets proposed by U.S. Department of Energy, reaching an ammonia yield rate above 1.0×10^{-6} mol cm^{-2} s^{-1} and a Faradaic efficiency above 90 %.[5]

Extensive efforts have been made to advance the electrochemical ammonia synthesis ($N_2 + 3H_2O \rightarrow 2NH_3 + 3/2O_2$).[6–14] Water splitting is a key step to provide hydrogen for nitrogen protonation ($*N_2 + 6H^+ + 6e^- \rightarrow * + 2NH_3$). Yan et al.[15] prepared VO_x with high concentration of oxygen vacancies, which promotes the water splitting and reduces the activation energy for nitrogen reduction. However, the poor selectivity of ammonia production via electrocatalytic nitrogen reduction still limits the industrialization potential. The poor selectivity is attributed to the fierce hydrogen evolution ($2H_2O + 2e^- \rightarrow H_2 + 2OH^-$), which is highly competitive with the nitrogen reduction.[16] In view of this, Au has been demonstrated as a promising

electrocatalyst for ammonia synthesis with high selectivity, benefiting from its weak side reaction of hydrogen evolution.[16] Another strategy to suppress the side reaction of hydrogen evolution is by controlling the transfer rate of protons via membrane design. Shen et al.[17] reported that the Faradaic efficiency of ammonia production can be regulated by tuning the pore numbers of polypropylene membrane. The pore numbers of membrane have a decisive effect on the transfer rate of protons, which are key reactants for nitrogen protonation, thus regulating the Faradaic efficiency of ammonia production. Resultantly, a high Faradaic efficiency of 41.86 % can be achieved when using a membrane with a pore area of 7.85×10^{-5} cm^2 in an H-type cell. Additionally, electrolyte also plays a critical role in determining the reaction environment of the electrode, thereby influencing the ammonia production performance.[3,18–23] For example, electrolyte counter-ion composition plays a key role in affecting the local reaction environment. Yan et al.[24] reported a strategy to greatly improve the selectivity of ammonia production by using electrolytes containing K^+ cations. Compared to other cations including Li^+, Na^+ and Cs^+, K^+ can regulate proton transfer from the bulk solution to the catalyst surface and promote proton-coupled electron transfer process by stabilizing the key intermediates, thus boosting the ammonia yield rate and selectivity. Although promises, the demand of water splitting for providing hydrogen often leads to sluggish protonation step ($*N_2 + 8H_2O + 6e^- \rightarrow * + 2NH_3 \cdot H_2O + 6OH^-$), thus causing a poor ammonia yield rate.[20]

In this work, nitrogen will react with H_3O^+ cations for ammonia production ($N_2 + 6H_3O^+ + 6e^- \rightarrow 2NH_3 \cdot H_2O + 4H_2O$) in alkaline media. The presence of H_3O^+ cations promotes the nitrogen protonation, avoiding the sluggish water splitting process. A home-made dual-layer electrode is prepared by spraying the commercial Au/C nanoparticles on carbon cloth, serving as the working electrode for nitrogen reduction to ammonia in a H-type cell. The reason we choose Au/C nanoparticles as the electrocatalyst is due to their commercial avialblity, superior ammonia production performance and long-term stability.[25] The effect of the anion in the

electrolyte on the nitrogen reduction is firstly investigated. Since the charge number of anions has a major impact on nitrogen reduction,[26] OH^-, Cl^- and SCN^- anions with one negative charge are selected. It is found that an ammonia yield rate is greatly boosted (6.69×10^{-11} mol cm^{-2} s^{-1}) with OH^- anions, compared to the anions of Cl^- (1.88×10^{-11} mol cm^{-2} s^{-1}) and SCN^- (1.14×10^{-11} mol cm^{-2} s^{-1}). The performance enhancement in the electrolyte containing the OH^- anions is possibly attributed to the appearance of hydronium ions (H_3O^+), which facilitates the dissociation of N_2 by strengthening protonation ($*N_2 + 6H_3O^+ + 6e^- \rightarrow * + 2NH_3\cdot H_2O + 4H_2O$). The appearance of H_3O^+ intermediates is induced by the presence of highly concentrated OH^- anions in the electrolyte (pH≥13), creating a unique acid-like local reaction environment.[27] While pH≤12, the protonation can be triggered only by water splitting ($*N_2 + 6H_2O + 6e^- \rightarrow * + 2NH_3 + 6OH^-$), which is kinetically sluggish and requires a large overpotential.[28] To further confirm this result, nitrogen reduction properties on the as-prepared electrode are investigated in the electrolytes containing different types of anions (1.0 M). For OH^- anions, an onset potential of -0.20 V for nitrogen reduction is required, more positive than that of Cl^- (-0.45 V) and SCN^- (-0.65 V). In addition, current densities contributed by nitrogen reduction reaction (j_{NRR}) are recorded in the electrolytes containing OH^- anions (11≤pH≤14) at an applied current or potential. It is found that j_{NRR} achieved by containing highly concentrated OH^- anions (pH≥13) shows around three-fold increase compared to those containing dilute OH^- anions (11≤pH≤12). This indicates that the appearance of H_3O^+ cations facilitates the nitrogen reduction. Last, such an enhancement is also observed on another electrode prepared by spraying the commercial Pd/C nanoparticles on carbon cloth. In the electrolyte containing 1.0 M OH^- anions, an ammonia yield rate of 3.23×10^{-11} mol cm^{-2} s^{-1} is achieved, much higher than those achieved by containing Cl^- (1.26×10^{-11} mol cm^{-2} s^{-1}) or SCN^- anions (0.82×10^{-11} mol cm^{-2} s^{-1}). Therefore, it is concluded that the appearance of H_3O^+ cations rendered by highly concentrated OH^- anions lowers the energy barrier for nitrogen reduction and promotes the

ammonia production performance. This work provides insights on nitrogen protonation step by H_3O^+ cations, which may guide the future electrolyte designs for efficient ammonia synthesis.

2. Experimental sections

2.1 Pretreatment of materials and electrode preparation

The effect of electrolyte anions on nitrogen reduction properties was investigated in an H-type cell by constructing a three-electrode system. The cathode, i.e., the working electrode for electrocatalytic nitrogen reduction, was prepared by spraying the ink made of commercial Au/C catalyst (Figure S1) onto a strip of carbon cloth (HESEN, Shanghai).The catalyst ink was prepared by mixing 60 wt. % Au/C (Premetek Co., USA) with 5 wt. % Nafion. The mixture was well dispersed in absolute ethanol by ultrasonication for at least 30 min. Then, the catalyst ink was sprayed onto the carbon cloth and dried, with a mass loading of 1.6 mg_{Au} cm^{-2} and a geometric active surface area of 1.0 × 1.0 cm^2. The Pd/C catalyst ink was also prepared by mixing 10 wt. % Pd/C with 5 wt. % Nafion, followed by spraying onto the carbon cloth, with a mass loading of 1.2 mg_{Pd} cm^{-2}. Graphite rod was used as the anode for oxygen evolution reaction and Ag/AgCl electrode was used as the reference electrode for accurately measuring the potential of the cathode. Nafion 115 membrane with a thickness of 125 μm was used to separate anode and cathode chamber. It was pretreated by boiled in 1.0 M KOH for 2 hours, followed by boiled in deionized water for 2 hours. The electrolyte in each chamber was kept at 100.0 mL.

2.2 Electrochemical measurements

All potentials were converted to reversible hydrogen electrode (RHE) by the following equations[29]:

$$E_{RHE} = E_{Ag/AgCl} + 0.059\mathrm{pH} + 0.197 \quad (1)$$

During cell operation, the cathodic reaction can be expressed[20]:

$$N_2 + 8H_2O + 6e^- \rightarrow 2NH_3{\cdot}H_2O + 6OH^- \qquad E^c = 0.092 \text{ V vs. RHE} \qquad (2)$$

The anodic reaction is the oxygen evolution reaction[30]:

$$6OH^- \rightarrow 3H_2O + 6e^- + 3/2O_2 \qquad E^a = 1.23 \text{ V vs. RHE} \qquad (3)$$

Hence, the overall reaction can be expressed:

$$N_2 + 5H_2O \rightarrow 2NH_3{\cdot}H_2O + 3/2O_2 \qquad E^0 = 1.138 \text{ V vs. RHE} \qquad (4)$$

At cathode inlet, an acid trap containing 0.05 M H_2SO_4 was used to remove the ammonia impurity from the N_2 gas source (99.995 vol. %). In addition, an alkaline trap containing 0.05 M NaOH was also added at cathode inlet to remove the NO_x impurity from the N_2 gas source. The NO_x impurity can be easily transformed to NO_2^- by the following reaction:

$$N_2O_3 + H_2O(l) \rightarrow HNO_2(aq) \qquad (5)$$

$$HNO_2(g) + H_2O(l) \rightarrow HNO_2(aq) + H_2O(l) \qquad (6)$$

$$2NO_2(g) + H_2O(l) \rightarrow HNO_2(aq) + HNO_3(aq) \qquad (7)$$

$$N_2O_4(g) + H_2O(l) \rightarrow HNO_2(aq) + HNO_3(aq) \qquad (8)$$

And NO_2^- can be much more easily reduced to ammonia or hydrazine compared to nitrogen, resulting in inaccurate quantification of ammonia production arising from nitrogen reduction.[22] At cathode outlet, a liquid seal was used to protect the ammonia contamination from the air. Electrochemical measurements were conducted by using Multi-Autolab electrochemical workstation (M204, Switzerland). 0.1 M potassium phosphate buffer (pH = 7.0) was prepared by mixing 61.5 mL K_2HPO_4 (1.0 M) and 38.5 mL KH_2PO_4 (1.0 M). KCl, KSCN and KOH electrolytes with a concentration of 1.0 M were prepared for investigating the anion effect on nitrogen reduction. Before cell construction, all components of the H-type cell were carefully washed by deionized water to remove the adsorbed ammonia or NO_x gases from the air. Before cell operation, N_2 or Ar gas was bubbled into the cathode chamber for 30 min to exhaust the residual air. During cell operation, the gas flow rate was kept at 20.0 sccm, which is controlled by a gas flowmeter. Additionally, the electrolyte in cathode chamber was stirred with a rate of

200 r min^{-1} to make dissolved nitrogen gas well dispersed. After cell operation, the solution in the cathode chamber was collected and mixed with colorimetric agent for ammonia detection. As for the cyclic test, the cathode was taken out after test and washed carefully using dilute sulfuric acid (0.001 M) and deionized water to remove the adsorbed ammonia on the cathode.

2.3 Detection and quantification of ammonia

The detection and quantification of ammonia in KCl and KSCN electrolyte were achieved by using Nessler's method.[2] The chromogenic solution was prepared by mixing 2.0 mL test solution, 0.2 mL potassium sodium tartrate (0.2 M) and 0.2 mL Nessler's reagent, in which sodium tartrate serve as the stabilizer for the chromogenic reaction:

$$NH_4^+ + 4OH^- + 2[HgI_4]^{2-} \rightarrow HgO{\cdot}Hg(NH_2)I\downarrow + 7I^- + 3H_2O \quad (9)$$

The mixed solution was stirred and rested for 20 min before the measurement of absorbance. The color development of the test solution was measured by recording the adsorption intensity at 420 nm using UV-Vis double beam spectrophotometer (DB-20, Australia). The detection and quantification of ammonia in KOH electrolyte were achieved by the indophenol blue method.[31–34] For the preparation of chromogenic agent, 1.0 mL solution containing 1.0 M NaOH, salicylic acid (3.0 wt. %) and sodium citrate (3.0 wt. %) was mixed with 0.5 mL sodium hypochlorite solution (5.0 wt. %) and 0.1 mL sodium nitroferricyanide dihydrate (1.0 wt. %). Then, 1.0 mL test solution was further added and rested for 2 hours for color development. The intensity of absorbance peak was measured at around 652 nm. As for the measurement of standard adsorption curves of different electrolytes, ammonia chloride electrolyte with certain concentrations (0.03125, 0.0625, 0.125, 0.25, 0.5, and 1.0 mg/L) was prepared and mixed with chromogenic agents for adsorption tests.

3. Results and discussion

An H-type cell containing a three-electrode system is constructed for the evaluation of nitrogen reduction properties and ammonia production performance, as shown in Figure S2. Nitrogen

reduction will take place in two-phase boundaries (interface between solid electrode and liquid electrolyte). In this work, the ammonia production is conducted in an H-type cell, in which the cathode for nitrogen reduction is completely immersed in the liquid electrolyte. The gaseous nitrogen will be first dissolved into the electrolyte via bubbling and then diffuse to the electrode surface for nitrogen reduction. To reveal the voltage window for nitrogen reduction, linear scan voltammetry (LSV) curves are measured in electrolytes saturated with Ar or N_2 gas. An additional current is observed in the N_2-saturated electrolyte when negatively scanning the applied potential from 0.0 V to -1.0 V, as shown in Figure 1. The current densities recorded in Ar-saturated electrolytes are contributed by the hydrogen evolution, which will occur when the applied potential is below thermodynamic equilibrium potential for hydrogen evolution (0.0 V vs. RHE). As for the current densities recorded in N_2-saturated electrolytes, it is contributed by the hydrogen evolution and nitrogen reduction, which will also occur when the applied potential is below the thermodynamic equilibrium potential of nitrogen reduction (0.092 V vs. RHE). Hence, the additional current in N_2-saturated electrolytes is contributed by the nitrogen reduction, thus enabling the identification of the voltage window for nitrogen reduction. First , the cell is operated in different electrolytes (KOH, KCl and KSCN) with a concentration of 1.0 M. It is found that the onset potential of -0.20 V for nitrogen reduction in the KOH electrolyte is observed (Figure 1a), much more positive than that in the KCl electrolyte (-0.45 V) and KSCN electrolyte (-0.65 V). Meanwhile, the current densities in the KOH electrolyte contributed by hydrogen evolution are significantly larger than those in the KCl electrolyte or KSCN electrolyte, indicating that the hydrogen evolution is also enhanced with the presence of OH^- anions. This is attributed to the anomalous hydrogen evolution behavior in high-pH environment, in which the generation of hydronium ions leads to an enhancement of hydrogen evolution.[27] The current density contributed by nitrogen reduction, i.e., j_{NRR}, is an important

indicator for the evaluation of nitrogen reduction capabilities, which can be calculated by the following equation:

$$j_{NRR} = j_T(Ar) - j_T(N_2) \quad (10)$$

Where j_T(Ar) represents the total current density recorded in Ar-saturated electrolytes, j_T(N_2) represents the total current density recorded in N_2-saturated electrolytes. As shown in Figure 1b, j_{NRR} in the KOH electrolyte reaches a maximum value of 1.82 mA cm^{-2} at -0.55 V vs. RHE, much higher than those in the KCl electrolyte (0.21 mA cm^{-2}) or in the KSCN electrolyte (0 mA cm^{-2}). In addition, reaching the maximum j_{NRR} requires a more negative potential in the KCl electrolyte (-0.70 V) or in the KSCN electrolyte (-0.80 V). These results confirm the excellent nitrogen reduction properties in the KOH electrolyte. The effect of anion type is further investigated by controlling pH in 0.1 M potassium phosphate buffer (pH = 7.0), as shown in Figures 1c-e. KOH, KCl and KSCN with a concentration of 0.01 M were individually added into the buffer, and the pH of each electrolyte maintains at 7.0. It was found that the onset potentials for nitrogen reduction with the presence of different anions are very close, showing an order of SCN^- (-0.476 V) < Cl^- (-0.474 V) < OH^- (-0.470 V), which follows the same order as nitrogen reduction in KSCN, KCl and KOH electrolytes (Figure 1a). Hence, the performance enhancement in the KOH electrolyte is mainly contributed by the high pH, and secondarily contributed by the type of OH^- anions. We believe the enhancement induced by high pH is mainly attributed to the generation of H_3O^+ cations in alkaline media during cell operation,[27] which facilitates the dissociation of $*N_2$ by strengthening protonation ($*N_2 + 6H_3O^+ + 6e^- \rightarrow * + 2NH_3 \cdot H_2O + 4H_2O$). With a large amount of OH^- anions, water splitting will be promoted due to the enhanced OH^- adsorption on the surface of the electrode. This leads to the generation of a large amount of *H via water splitting in alkaline electrolyte ($H_2O + e^- \rightarrow *H + OH^-$). The surface of the electrode within the electric double layer (EDL) will be soon

covered with *H in the form of underpotential deposition of hydrogen (H_{upd}) due to the strong binding effect between the H_{upd} and Au, as shown in Figure 2a. As water splitting proceeds, more and more *H start to combine with water molecules due to the limited active sites for H_{upd} on the surface of the electrode, forming free H_3O^+ cations within the EDL (Figure 2b). The other dissociation product (OH^-) will directly desorb out of the EDL by forming a hydroxyl-water-alkali metal cation adduct, i.e., $OH^*\text{-}(H_2O)_n\text{-}K^+$, and diffuse into the bulk solution. Hence, a large amount of H_3O^+ cations will be present within the EDL, without reacting with the OH^- anions. These free H_3O^+ cations will serve as the reactants for dissociation of $*N_2$, which is previously adsorbed on the surface of the electrode ($* + N_2 \rightarrow *N_2$). The supply of H_3O^+ cations within the EDL facilitates the protonation step ($*N_2 + 6H_3O^+ + 6e^- \rightarrow * + 2NH_3 \cdot H_2O + 4H_2O$), forming ammonia hydrate and releasing water molecules, thus improving the ammonia yield rate. As for the cell operation in KCl electrolyte or KSCN electrolyte, the presence of low-concentration OH^- anions (10^{-7} M) results in sluggish water splitting as compared to that in the electrolyte containing OH^- anions (1.0 M). Therefore, only a small amount of *H will be generated within EDL, which will be quickly transferred to H_{upd} and be strongly bonded at the surface of the electrode. These *H will not combine with water molecules, thus generating no H_3O^+ cations during this process (Figure 2e). As a result, the protonation of $*N_2$ will be only triggered by water splitting ($*N_2 + 6H_2O + 6e^- \rightarrow * + 2NH_3 + 6OH^-$), which is more kinetically sluggish (Figure 2f).

To further confirm this result, the ammonia production performance is evaluated in different electrolytes by operating the cell at an applied current or potential. The quantification of ammonia product is achieved by colorimetric methods, and the standard adsorption curves of NH_4^+ in the KOH electrolyte (Figure S3), the KCl electrolyte (Figure S4) and the KSCN electrolyte (Figure S5) are measured. All curves show good linear fits ($R^2 \geq 0.999$) between the absorbance and ammonia concentrations. The comparison tests are first conducted to

eliminate the possible ammonia contamination during the cell operation. It is found that adding an acid trap can effectively eliminate the ammonia contamination from the nitrogen source, with no observation of UV adsorption peak at 652 nm, which is the characteristic peak of ammonia products (Figure S6). In comparison, bubbling nitrogen into the cell without acid traps for 2 hours will lead to ammonia contamination, observing a distinct UV adsorption peak at 652 nm. In addition, cell operation at open-circuit condition displays no adsorption peak at 652 nm, indicating the cell system is well sealed and the cell components are cleaned up, without the introduction of ammonia contamination. Cell operation under Ar condition at -0.5 V also displays no distinct absorbance peak intensity, in sharp contrast to the cell operation under N_2 condition with an absorbance intensity of 0.037, confirming that ammonia products result from the reduction of introduced N_2 gas. Therefore, it is concluded that there is no ammonia contamination during cell operation and the quantification of ammonia products resulted from electrochemical nitrogen reduction is accurate.

The ammonia yield rate is calculated by the following equation[19]:

$$r_{NH3} = (n \times V)/(t \times A) \quad (11)$$

Where r_{NH3} stands for the ammonia yield rate, n is the ammonia concentration, V represents the volume of the electrolyte, t is the reaction time, and A is the geometric area of electrodes (2×2 cm^2) immersed in the electrolyte.

The Faradaic efficiencies are calculated by the following equation[19]:

$$FE\ (\%) = (3F \times n \times V)/(M \times Q) \quad (12)$$

Where n is the ammonia concentration, V stands for the volume of the electrolyte (100.0 mL), M is the relative molecular mass of NH_3, and Q represents the total charge used during cell operation.

As shown in Figure 3a, at a current density of -10 mA cm^{-2}, the potential is around -0.30 V in the KOH electrolyte, more positive than those of in the KCl electrolyte (-0.71 V) or in the KSCN electrolyte (-0.83 V). The resultant ammonia production performance in the KOH electrolyte is 9.39×10^{-11} mol cm^{-2} s^{-1}, higher than in the KCl electrolyte (4.33×10^{-11} mol cm^{-2} s^{-1}) or in the KSCN electrolyte (7.02×10^{-11} mol cm^{-2} s^{-1}), as shown in Figure 3c. This indicates that the presence of OH^- anions improves the ammonia yield rate and reduces the consumption of electric energy. At an applied potential of -0.6 V, cell operation in the KOH electrolyte displays much larger current densities around 55.0 mA cm^{-2} (Figure 3b), as compared to that in the KCl electrolyte (~4.27 mA cm^{-2}) and in the KSCN electrolyte (~1.35 mA cm^{-2}). The resultant ammonia production performance in the KOH electrolyte (6.69×10^{-11} mol cm^{-2} s^{-1}) is much more superior than that in the KCl electrolyte (1.88×10^{-11} mol cm^{-2} s^{-1}) or in the KSCN electrolyte (1.14×10^{-11} mol cm^{-2} s^{-1}), as shown in Figure 3d, Figure S7 and Figure S8. This further confirms the improvement of the ammonia production performance in the electrolyte containing OH^- anions, which is attributed to the enhanced protonation by reacting with H_3O^+ cations.

The ammonia production capabilities are further investigated by measuring LSV curves in the KOH electrolytes with different OH^- concentrations, as shown in Figure 4a. It is found that the hydrogen evolution in the electrolyte with a higher pH value outperforms that in the electrolyte with a lower one, which is also attributed to the presence of H_3O^+ cations in high-pH environment (pH $\geq$ 13) during cell operation. The onset potential for nitrogen reduction in electrolytes with different pH values is calculated (Figure 4b). It is found that the onset potentials in high-pH environment (pH $\geq$ 13) are more positive than those in low-pH environment (11$\leq$ pH $\leq$12), displaying a reduced energy barrier of nitrogen reduction. In low-pH environment (pH $\leq$12), limited OH^- ions ($\leq$ 0.01 M) are available in the electrolyte, showing small adsorption energy with low coverage of oxygen,[35] thus resulting in sluggish water

splitting. Limited *H will be generated during water splitting, which will be attached on the surface of the electrode and combine with each other to produce H_2 via a Tafel reaction (*H + *H → H_2).[27] Hence, there is no generation of H_3O^+ cations during water splitting. In addition, j_{NRR} in high-pH environment (with H_3O^+ cations) are about three-fold increases compared to those in low-pH environment (without H_3O^+ cations) at an applied current of -10.0 mA cm^{-2} (Figure 4c) or at an applied potential of -0.5 V (Figure 4d). These experimental results perfectly match with our previous belief, i.e., H_3O^+ cations facilitate the nitrogen reduction to ammonia. To further confirm the viewpoint of performance enhancement in alkaline media by generating H_3O^+ cations, nitrogen reduction properties of Pd/C nanoparticles in different electrolytes are investigated. LSV curves (Figure S9) show that the onset potential in the KOH electrolyte is -0.52 V, more positive than those in the KCl electrolyte (-0.78 V) and KSCN electrolyte (-0.64 V). The observation of reduced energy barrier for nitrogen reduction in the KOH electrolyte on the electrode made of Pd/C nanoparticles is consistent with that on the electrode made of Au/C nanoparticles. In addition, the ammonia yield rate in the KOH electrolyte (3.23×10^{-11} mol cm^{-2} s^{-1}) is also much larger than those in the KCl electrolyte (0.82×10^{-11} mol cm^{-2} s^{-1}) and the KSCN electrolyte (1.26×10^{-11} mol cm^{-2} s^{-1}) when operating the cell at a given potential of -0.8 V (Figure S10). These results further demonstrate the ammonia production can be boosted with the presence of OH^- anions.

Lastly, the ammonia production rates in the KOH electrolyte (1.0 M) at different potentials are measured, as shown in Figure 5. At an applied potential of -0.35 V (vs. RHE), it displays a low ammonia yield rate of 4.82×10^{-11} mol cm^{-2} s^{-1}. The ammonia yield rate increases at a more negative potential, resulting in an ammonia yield rate of 2.11×10^{-10} mol cm^{-2} s^{-1} at -0.5 V (vs. RHE). Subsequently, the rate decreases at a more negative potential, due to the enhanced side reaction of hydrogen evolution. The stable ammonia yield rates during intermittent cycles with

Ar or N_2 flow at -0.5 V demonstrate that the cathode can be reversibly used for ammonia production.

4. **Concluding remarks**

In summary, the effect of anions in the electrolyte composition on electrocatalytic nitrogen reduction to ammonia is investigated. It is found that the presence of OH^- anions greatly boosts the ammonia production performance (6.69×10^{-11} mol cm^{-2} s^{-1}) as compared to other anions including Cl^- (1.18×10^{-11} mol cm^{-2} s^{-1}) and SCN^- anions (1.14×10^{-11} mol cm^{-2} s^{-1}). It also reduces the energy barrier, displaying the most positive onset potential of -0.2 V for nitrogen reduction among three types of anions. Such enhancement is possibly attributed to the appearance of hydronium ions in alkaline media, which facilitates nitrogen reduction to ammonia by strengthening protonation ($*N_2 + 6H_3O^+ + 6e^- \rightarrow * + 2NH_3 \cdot H_2O + 4H_2O$). This work provides a new approach to tailor local reaction environment of the electrode for promoting nitrogen reduction to ammonia.

Conflicts of interest:

There are no conflicts to declare.

Acknowledgement:

This work is supported by a grant from the Research Grants Council of the Hong Kong Special Administrative Region, China (Project No. 15222018) and a grant from The Hong Kong Polytechnic University (1-ZE30).

References

(1) Medford, A. J.; Hatzell, M. C. Photon-Driven Nitrogen Fixation: Current Progress, Thermodynamic Considerations, and Future Outlook. *ACS Catal.* **2017**, *7* (4), 2624–2643. https://doi.org/10.1021/acscatal.7b00439.

(2) Zhao, Y.; Shi, R.; Bian, X.; Zhou, C.; Zhao, Y.; Zhang, S.; Wu, F.; Waterhouse, G. I. N.; Wu, L. Z.; Tung, C. H.; et al. Ammonia Detection Methods in Photocatalytic and Electrocatalytic Experiments: How to Improve the Reliability of NH 3 Production Rates? *Adv. Sci.* **2019**, *6* (8), 1802109. https://doi.org/10.1002/advs.201802109.

(3) Guo, X.; Du, H.; Qu, F.; Li, J. Recent Progress in Electrocatalytic Nitrogen Reduction. *J. Mater. Chem. A* **2019**, *7* (8), 3531–3543. https://doi.org/10.1039/c8ta11201k.

(4) Légaré, M. A.; Bélanger-Chabot, G.; Dewhurst, R. D.; Welz, E.; Krummenacher, I.; Engels, B.; Braunschweig, H. Nitrogen Fixation and Reduction at Boron. *Science (80-.).* **2018**, *359* (6378), 896–900. https://doi.org/10.1126/science.aaq1684.

(5) Tang, C.; Qiao, S. Z. How to Explore Ambient Electrocatalytic Nitrogen Reduction Reliably and Insightfully. *Chem. Soc. Rev.* **2019**, *48* (12), 3166–3180. https://doi.org/10.1039/c9cs00280d.

(6) Wang, S.; Wei, W.; Lv, X.; Huang, B.; Dai, Y. W Supported on G-CN Manifests High Activity and Selectivity for N2 Electroreduction to NH3. *J. Mater. Chem. A* **2020**, *8* (3), 1378–1385. https://doi.org/10.1039/c9ta10935h.

(7) Lai, F.; Feng, J.; Ye, X.; Zong, W.; He, G.; Yang, C.; Wang, W.; Miao, Y. E.; Pan, B.; Yan, W.; et al. Oxygen Vacancy Engineering in Spinel-Structured Nanosheet Wrapped

Hollow Polyhedra for Electrochemical Nitrogen Fixation under Ambient Conditions. *J. Mater. Chem. A* **2020**, *8* (4), 1652–1659. https://doi.org/10.1039/c9ta11408d.

(8) Lai, F.; Chen, N.; Ye, X.; He, G.; Zong, W.; Holt, K. B.; Pan, B.; Parkin, I. P.; Liu, T.; Chen, R. Refining Energy Levels in ReS2 Nanosheets by Low-Valent Transition-Metal Doping for Dual-Boosted Electrochemical Ammonia/Hydrogen Production. *Adv. Funct. Mater.* **2020**, *1907376*, 1–9. https://doi.org/10.1002/adfm.201907376.

(9) Tong, W.; Huang, B.; Wang, P.; Li, L.; Shao, Q.; Huang, X. Crystal-Phase-Engineered PdCu Electrocatalyst for Enhanced Ammonia Synthesis. *Angew. Chemie - Int. Ed.* **2020**, *59* (7), 2649–2653. https://doi.org/10.1002/anie.201913122.

(10) Hao, Q.; Liu, C.; Jia, G.; Wang, Y.; Arandiyan, H.; Wei, W.; Ni, B. J. Catalytic Reduction of Nitrogen to Produce Ammonia by Bismuth-Based Catalysts: State of the Art and Future Prospects. *Mater. Horizons* **2020**, *7* (4), 1014–1029. https://doi.org/10.1039/c9mh01668f.

(11) Sun, Y.; Deng, Z.; Song, X. M.; Li, H.; Huang, Z.; Zhao, Q.; Feng, D.; Zhang, W.; Liu, Z.; Ma, T. Bismuth-Based Free-Standing Electrodes for Ambient-Condition Ammonia Production in Neutral Media. *Nano-Micro Lett.* **2020**, *12* (1), 133–145. https://doi.org/10.1007/s40820-020-00444-y.

(12) Li, G.; Yu, Y.; Pan, Z.; An, L. Two-Dimensional Layered SnO2 Nanosheets for Ambient Ammonia Synthesis. *ACS Appl. Energy Mater.* **2020**, *3* (7), 6735–6742. https://doi.org/10.1021/acsaem.0c00858.

(13) Mukherjee, S.; Yang, X.; Shan, W.; Samarakoon, W.; Karakalos, S.; Cullen, D. A.; More, K.; Wang, M.; Feng, Z.; Wang, G.; et al. Atomically Dispersed Single Ni Site Catalysts for Nitrogen Reduction toward Electrochemical Ammonia Synthesis Using N2 and H2O. *Small Methods* **2020**, *4* (6), 1900821. https://doi.org/10.1002/smtd.201900821.

(14) Liu, Y.; Esan, O. C.; Pan, Z.; An, L. Machine Learning for Advanced Energy Materials. *Energy AI* **2021**, *3*, 100049. https://doi.org/https://doi.org/10.1016/j.egyai.2021.100049.

(15) Fang, W.; Zhao, J.; Wu, T.; Huang, Y.; Yang, L.; Liu, C.; Zhang, Q.; Huang, K.; Yan, Q. Hydrophilic Engineering of VO: X-Based Nanosheets for Ambient Electrochemical Ammonia Synthesis at Neutral PH. *J. Mater. Chem. A* **2020**, *8* (12), 5913–5918. https://doi.org/10.1039/d0ta00676a.

(16) Li, M.; Huang, H.; Low, J.; Gao, C.; Long, R.; Xiong, Y. Recent Progress on Electrocatalyst and Photocatalyst Design for Nitrogen Reduction. *Small Methods* **2019**, *3* (6), 1800388. https://doi.org/10.1002/smtd.201800388.

(17) Liu, Y.; Zhang, X.; Chen, Z.; Zhang, X.; Tsiakaras, P.; Shen, P. K. Electrocatalytic Reduction of Nitrogen on FeAg/Si for Ammonia Synthesis: A Simple Strategy for Continuous Regulation of Faradaic Efficiency by Controlling H+ Ions Transfer Rate. *Appl. Catal. B Environ.* **2021**, *283* (June 2020), 119606. https://doi.org/10.1016/j.apcatb.2020.119606.

(18) Cui, X.; Tang, C.; Zhang, Q. A Review of Electrocatalytic Reduction of Dinitrogen to Ammonia under Ambient Conditions. *Adv. Energy Mater.* **2018**, *8* (22), 1–25. https://doi.org/10.1002/aenm.201800369.

(19) Chen, G.-F.; Ren, S.; Zhang, L.; Cheng, H.; Luo, Y.; Zhu, K.; Ding, L.-X.; Wang, H. Advances in Electrocatalytic N 2 Reduction-Strategies to Tackle the Selectivity Challenge . *Small Methods* **2019**, *3* (6), 1800337. https://doi.org/10.1002/smtd.201800337.

(20) Guo, W.; Zhang, K.; Liang, Z.; Zou, R.; Xu, Q. Electrochemical Nitrogen Fixation and Utilization: Theories, Advanced Catalyst Materials and System Design. *Chem. Soc. Rev.* **2019**, *48* (24), 5658–5716. https://doi.org/10.1039/c9cs00159j.

(21) Singh, A. R.; Rohr, B. A.; Schwalbe, J. A.; Cargnello, M.; Chan, K.; Jaramillo, T. F.; Chorkendorff, I.; Nørskov, J. K. Electrochemical Ammonia Synthesis - The Selectivity Challenge. *ACS Catal.* **2017**, *7* (1), 706–709. https://doi.org/10.1021/acscatal.6b03035.

(22) Suryanto, B. H. R.; Du, H. L.; Wang, D.; Chen, J.; Simonov, A. N.; MacFarlane, D. R. Challenges and Prospects in the Catalysis of Electroreduction of Nitrogen to Ammonia. *Nat. Catal.* **2019**, *2* (4), 290–296. https://doi.org/10.1038/s41929-019-0252-4.

(23) Liu, K. H.; Zhong, H. X.; Li, S. J.; Duan, Y. X.; Shi, M. M.; Zhang, X. B.; Yan, J. M.; Jiang, Q. Advanced Catalysts for Sustainable Hydrogen Generation and Storage via Hydrogen Evolution and Carbon Dioxide/Nitrogen Reduction Reactions. *Prog. Mater. Sci.* **2018**, *92* (4), 64–111. https://doi.org/10.1016/j.pmatsci.2017.09.001.

(24) Hao, Y. C.; Guo, Y.; Chen, L. W.; Shu, M.; Wang, X. Y.; Bu, T. A.; Gao, W. Y.; Zhang, N.; Su, X.; Feng, X.; et al. Promoting Nitrogen Electroreduction to Ammonia with Bismuth Nanocrystals and Potassium Cations in Water. *Nat. Catal.* **2019**, *2*, 448–456. https://doi.org/10.1038/s41929-019-0241-7.

(25) Wang, J.; Yu, L.; Hu, L.; Chen, G.; Xin, H.; Feng, X. Ambient Ammonia Synthesis via Palladium-Catalyzed Electrohydrogenation of Dinitrogen at Low Overpotential. *Nat. Commun.* **2018**, *9* (1). https://doi.org/10.1038/s41467-018-04213-9.

(26) Myers, D. Electrostatic Forces and the Electrical Double Layer. *Surfaces, Interfaces, and Colloids*. April 28, 2002, pp 79–96. https://doi.org/https://doi.org/10.1002/0471234990.ch5.

(27) Wang, X.; Xu, C.; Jaroniec, M.; Zheng, Y.; Qiao, S. Z. Anomalous Hydrogen Evolution Behavior in High-PH Environment Induced by Locally Generated Hydronium Ions. *Nat. Commun.* **2019**, *10* (1), 1–8. https://doi.org/10.1038/s41467-019-12773-7.

(28) Subbaraman, R.; Tripkovic, D.; Chang, K.-C.; Strmcnik, D.; Paulikas, A. P.; Hirunsit, P.; Chan, M.; Greeley, J.; Stamenkovic, V.; Markovic, N. M. Trends in Activity for the Water Electrolyser Reactions on 3d M(Ni,Co,Fe,Mn) Hydr(Oxy)Oxide Catalysts. *Nat. Mater.* **2012**, *11* (6), 550–557. https://doi.org/10.1038/nmat3313.

(29) Liu, Y.; Li, D.; Yu, J.; Ding, B. Stable Confinement of Black Phosphorus Quantum Dots on Black Tin Oxide Nanotubes: A Robust, Double-Active Electrocatalyst toward Efficient Nitrogen Fixation. *Angew. Chemie* **2019**, *131* (46), 16591–16596. https://doi.org/10.1002/ange.201908415.

(30) Tang, C.; Wang, H. Sen; Wang, H. F.; Zhang, Q.; Tian, G. L.; Nie, J. Q.; Wei, F. Spatially Confined Hybridization of Nanometer-Sized NiFe Hydroxides into Nitrogen-Doped Graphene Frameworks Leading to Superior Oxygen Evolution Reactivity. *Adv. Mater.* **2015**, *27* (30), 4516–4522. https://doi.org/10.1002/adma.201501901.

(31) Andersen, S. Z.; Čolić, V.; Yang, S.; Schwalbe, J. A.; Nielander, A. C.; McEnaney, J. M.; Enemark-Rasmussen, K.; Baker, J. G.; Singh, A. R.; Rohr, B. A.; et al. A Rigorous Electrochemical Ammonia Synthesis Protocol with Quantitative Isotope Measurements. *Nature* **2019**, *570* (7762), 504–508. https://doi.org/10.1038/s41586-019-1260-x.

(32) Zhang, X.; Kong, R. M.; Du, H.; Xia, L.; Qu, F. Highly Efficient Electrochemical Ammonia Synthesis: Via Nitrogen Reduction Reactions on a VN Nanowire Array under Ambient Conditions. *Chem. Commun.* **2018**, *54* (42), 5323–5325. https://doi.org/10.1039/c8cc00459e.

(33) Jin, H.; Li, L.; Liu, X.; Tang, C.; Xu, W.; Chen, S.; Song, L.; Zheng, Y.; Qiao, S. Z. Nitrogen Vacancies on 2D Layered W2N3: A Stable and Efficient Active Site for Nitrogen Reduction Reaction. *Adv. Mater.* **2019**, *31* (32), 1–8. https://doi.org/10.1002/adma.201902709.

(34) Chu, K.; Liu, Y. P.; Wang, J.; Zhang, H. NiO Nanodots on Graphene for Efficient Electrochemical N2 Reduction to NH3. *ACS Appl. Energy Mater.* **2019**, *2* (3), 2288–2295. https://doi.org/10.1021/acsaem.9b00102.

(35) Miller, S. D.; Inoğlu, N.; Kitchin, J. R. Configurational Correlations in the Coverage Dependent Adsorption Energies of Oxygen Atoms on Late Transition Metal Fcc(111) Surfaces. *J. Chem. Phys.* **2011**, *134* (10). https://doi.org/10.1063/1.3561287.

Figures:

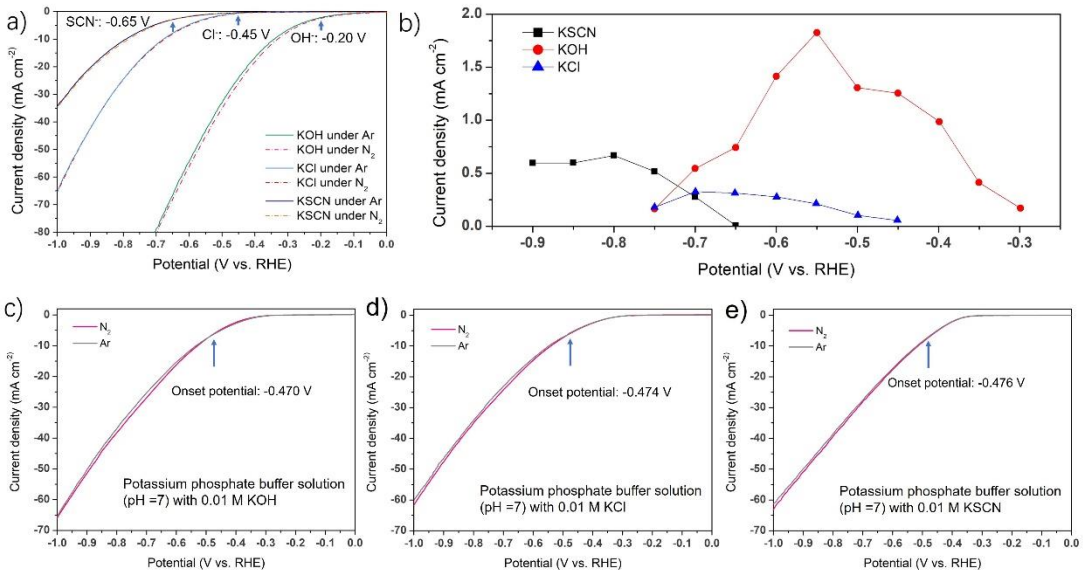

Figure 1 LSV curves in different electrolytes under the condition of Ar and N_2 gases. (a) KOH, KCl and KSCN electrolytes with a concentration of 1.0 M. The onset potentials for nitrogen reduction in different electrolytes are labeled. (b) Current densities contributed by nitrogen reduction in electrolytes with a concentration of 1.0 M. (c) Potassium phosphate buffer with the addition of 0.01 M KOH. (d) Potassium phosphate buffer with the addition of 0.01 M KCl. (e) Potassium phosphate buffer with the addition of 0.01 M KSCN.

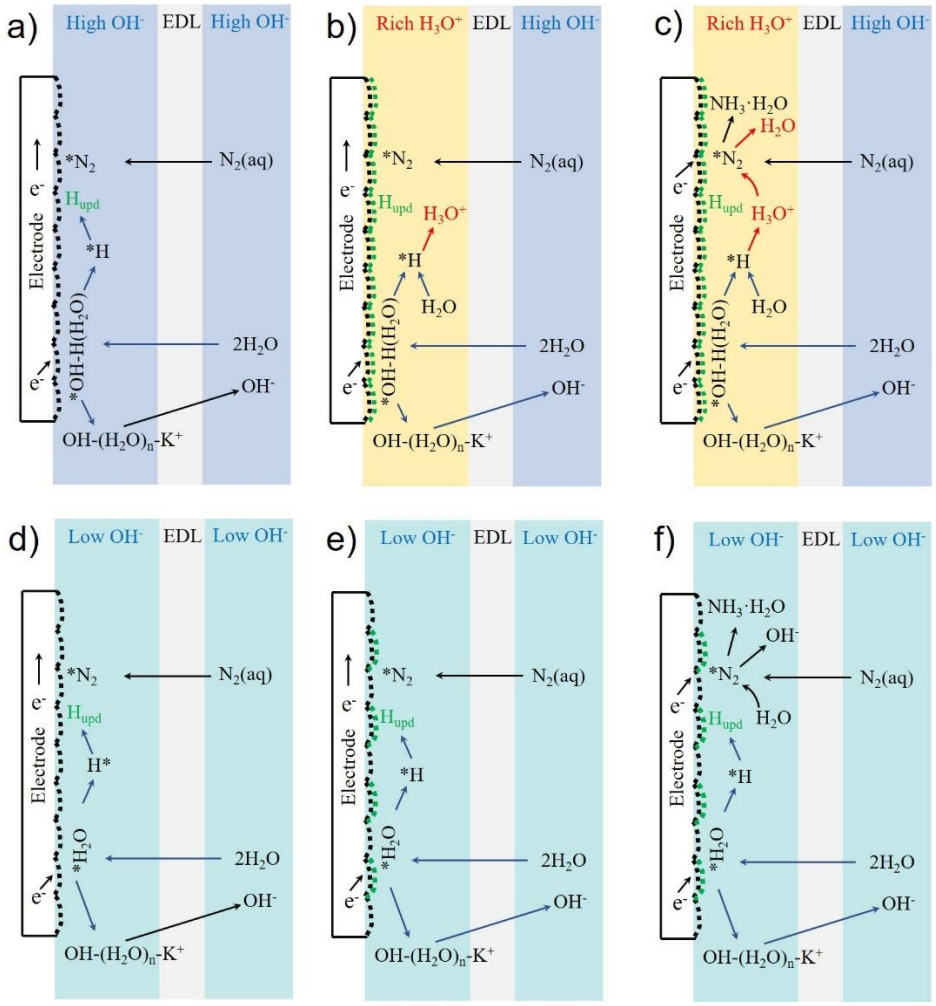

Figure 2 Schematic illustrations of nitrogen reduction in different media. (a-c) High-pH environment (pH≥13). (d-f) Low-pH environment (11≤pH≤12).

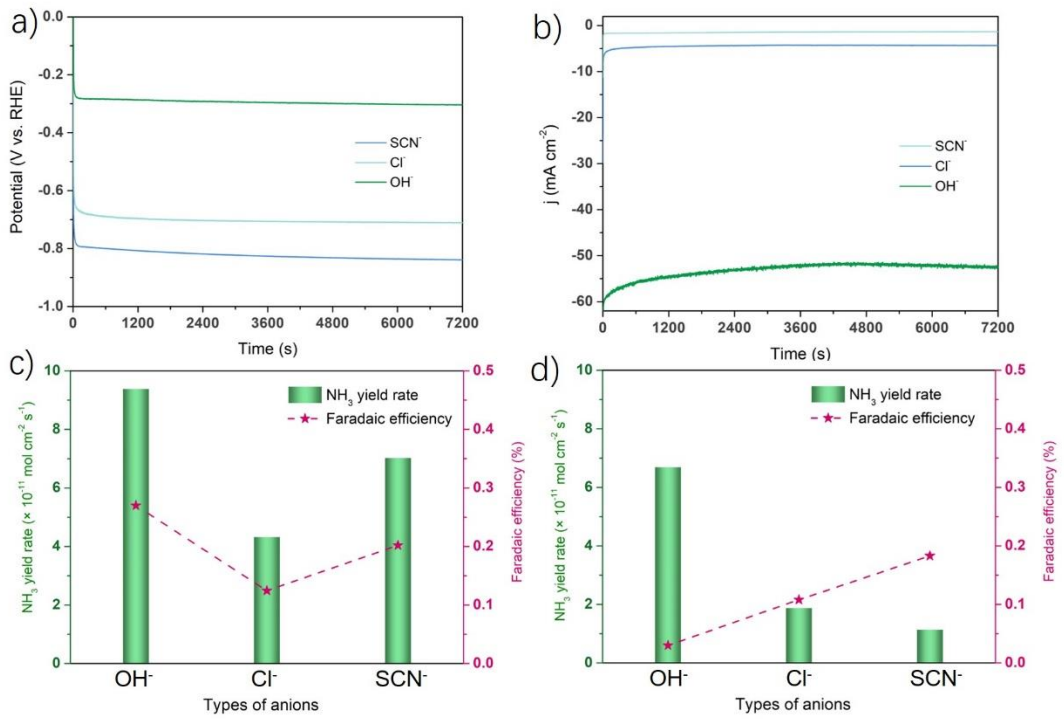

Figure 3 Electrocatalytic nitrogen reduction and corresponding ammonia production performance in electrolytes containing different anions. (a) V-t curves at a total current density of -10.0 mA cm^{-2}. (b) I-t curves at a potential of -0.6 V vs. RHE. Ammonia production performance (c) at a given total current density of -10.0 mA cm^{-2} and (d) at a given potential of -0.6 V vs. RHE.

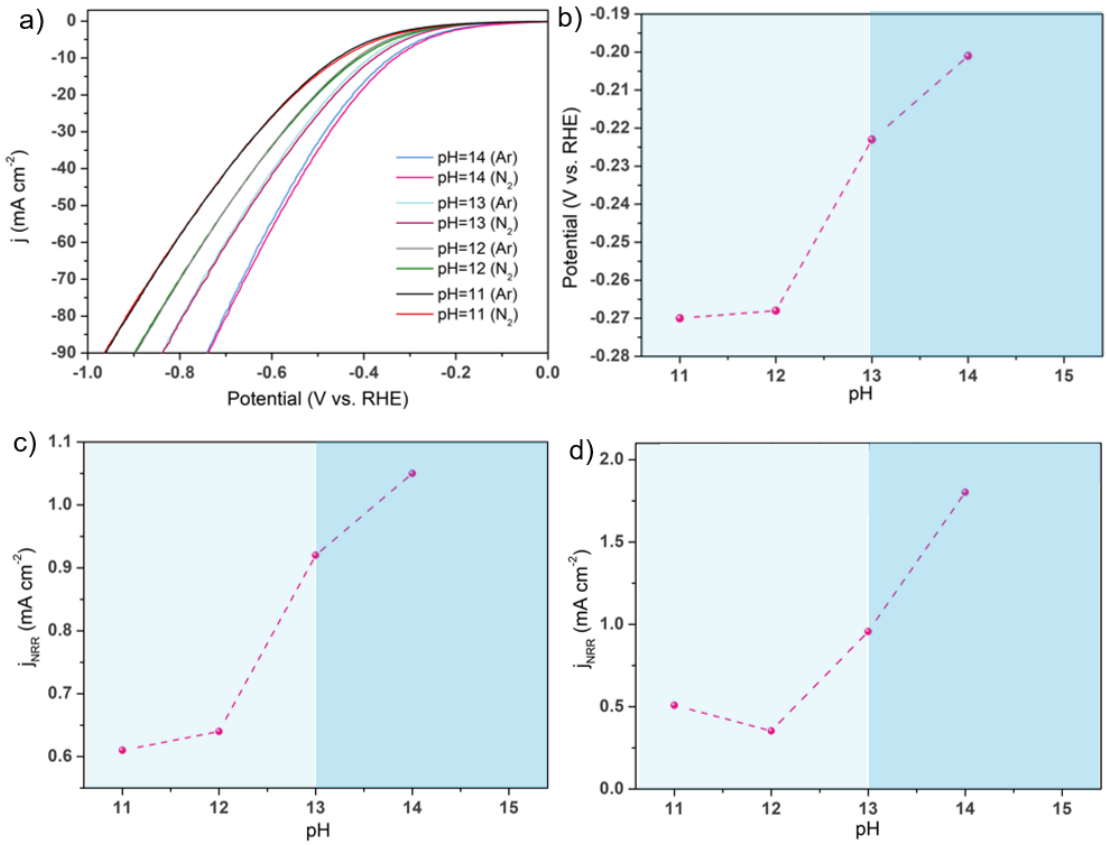

Figure 4 (a) LSV curves and (b) the onset potentials for nitrogen reduction at different pH values. (c) j_{NRR} at different pH values at a total current density of -10.0 mA cm^{-2}. (d) j_{NRR} at different pH values at -0.5 V vs. RHE.

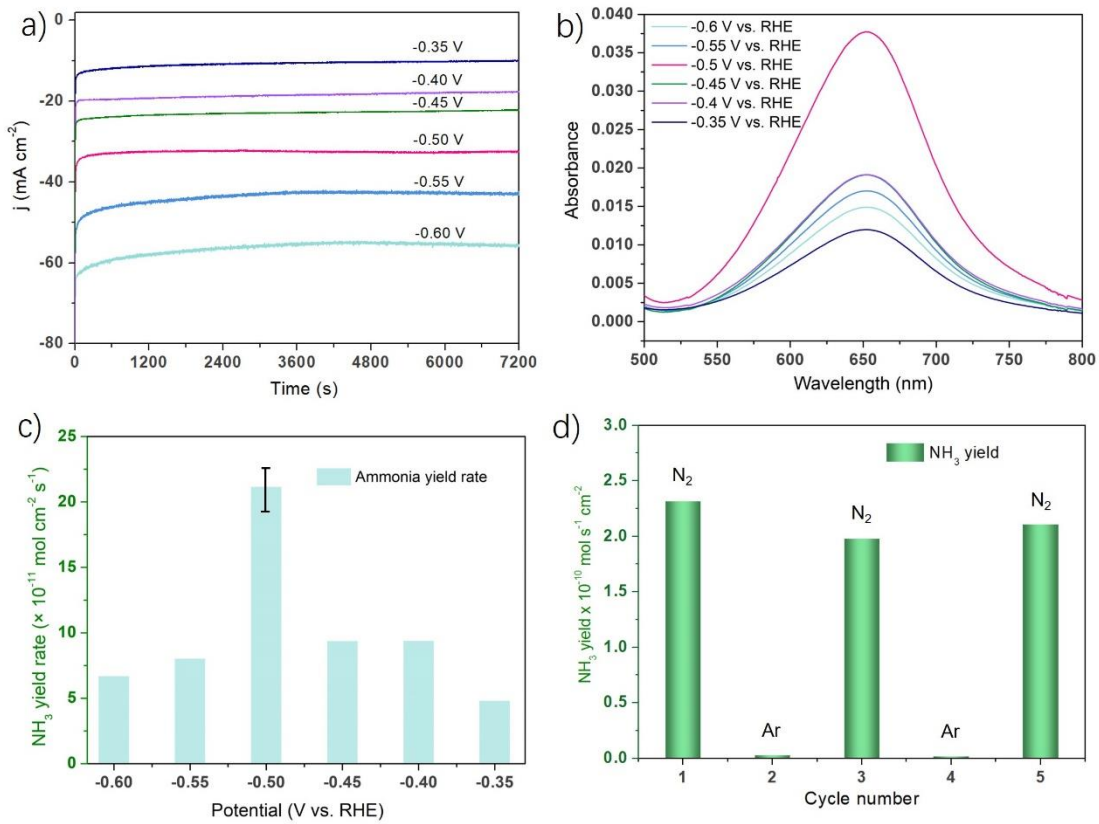

Figure 5 (a) I-t curves with a nitrogen flow. (b) UV adsorption curves for the detection of ammonia. (c) Ammonia yield rates. (d) Ammonia yield rates of intermittent cycles with Ar or N_2 flow at -0.5 V vs. RHE.